

# The Gradient Puppeteer: Adversarial Domination in Gradient Leakage Attacks through Model Poisoning

Kunlan Xiang<sup>1</sup> Haomiao Yang<sup>1</sup> Meng Hao<sup>2</sup> Haoxin Wang<sup>3</sup> Shaofeng Li<sup>4</sup> Zikang Ding<sup>1</sup> Tianwei Zhang<sup>5</sup>

## Abstract

In Federated Learning (FL), clients share gradients with a central server while keeping their data local. However, malicious servers could deliberately manipulate the models to reconstruct clients' data from shared gradients, posing significant privacy risks. Although such active gradient leakage attacks (AGLAs) have been widely studied, they suffer from several limitations including incomplete attack coverage and poor stealthiness. In this paper, we address these limitations with two core contributions. First, we introduce a new theoretical analysis approach, which uniformly models AGLAs as backdoor poisoning. This analysis approach reveals that the core principle of AGLAs is to bias the gradient space to prioritize the reconstruction of a small subset of samples while sacrificing the majority, which theoretically explains the above limitations of existing AGLAs. Second, we propose Enhanced Gradient Global Vulnerability (EGGV), the first AGLA that achieves complete attack coverage while evading client-side detection. In particular, EGGV employs a gradient projector and a jointly optimized discriminator to assess gradient vulnerability, steering the gradient space toward the point most prone to data leakage. Extensive experiments show that EGGV achieves complete attack coverage and surpasses SOTA with at least a 43% increase in reconstruction quality (PSNR) and a 45% improvement in stealthiness (D-SNR).

## 1. Introduction

Federated Learning (FL) (McMahan et al., 2017; Bonawitz et al., 2019; Chilimbi et al., 2014) allows multiple clients to collaboratively train a shared model without exchanging raw

<sup>1</sup>University of Electronic Science and Technology of China <sup>2</sup>Singapore Management University <sup>3</sup>Sichuan University <sup>4</sup>Southeast University <sup>5</sup>Nanyang Technological University. Correspondence to: Haomiao Yang <haomyang@uestc.edu.cn>.

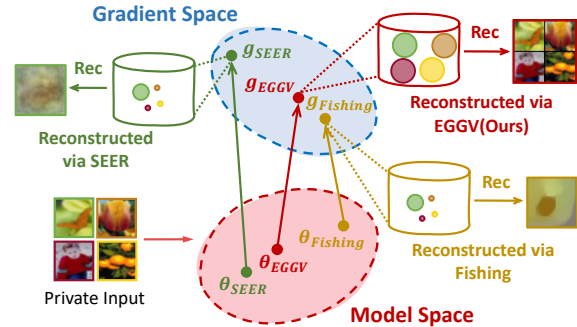


Figure 1. Illustration of the fundamental principles and reconstruction results of Fishing (Wen et al., 2022), SEER (Garov et al., 2024), and EGGV (Ours).

data. Despite avoiding direct data sharing, FL is vulnerable to Gradient Leakage Attacks (GLAs) (Zhu et al., 2019), where adversaries exploit shared gradients to reconstruct clients' data. These attacks are broadly categorized into two types (Nowak et al., 2024): Passive Gradient Leakage Attacks (PGLAs) (Zhu & Blaschko, 2021; Yang et al., 2022; Yue et al., 2023), and Active Gradient Leakage Attacks (AGLAs) (Boenisch et al., 2023; Zhao et al., 2023; Fowl et al., 2021; Nowak et al., 2024).

In PGLAs, attackers reconstruct client data from shared gradients without modifying the global model and the FL protocol. However, the effectiveness of these attacks heavily depends on the initialization of model parameters. Our experimental results in Table 1 and Figure 7 demonstrate that, for the first time, even previously considered effective PGLAs fail to reconstruct the data when improper initialization methods are used by attackers.

In contrast, in AGLAs, attackers achieve data reconstruction by modifying the model structure and parameters. Such attacks exhibit several limitations in term of attack stealthiness and coverage. Specifically, some AGLAs (Boenisch et al., 2023; Zhao et al., 2023; Fowl et al., 2021; Nowak et al., 2024) conduct direct and accurate reconstruction by inserting a fully connected layer in front of the model and modifying its parameters, which are evident to be detected by clients. Other AGLAs (Wen et al., 2022; Garov et al., 2024) improve PGLAs by reducing effective samples used for gradient computation, which can only reconstruct a few or even one sample, as shown in Figure 1.

This paper addresses the above critical challenges with two major contributions. First, we propose a new theoretical approach to rethinking and analyzing AGLAs. The core of our approach is the introduction of a parameter  $\lambda$ , which can quantify the relative contribution of each sample within a batch to the activation of neurons in each class. It discloses that the fundamental principle of existing AGLAs is to protoze the reconstruction of a small subset of samples with specific properties, while sacrificing the majority of other samples. Such properties are analogous to triggers in backdoor attacks. This principle explains the critical limitations of existing AGLAs, underscoring the pressing need for an advanced attack with a fundamentally different principle.

Second, based on the above theoretical analysis, we propose Enhanced Gradient Global Vulnerability (EGGV), a novel AGLA that ensures complete attack coverage and evades client-side detection. Different from existing attacks, EGGV equally enhances the gradient vulnerability of all samples in a batch, as illustrated in Figure 1. Its key insights include: (i) treating gradients as a latent space of data, with the forward and backward propagation of the model as an encoding process; (ii) introducing a discriminator jointly trained with the model to access the gradient vulnerability of the model. Importantly, EGGV opens up a new research path thoroughly different from gradient-biased AGLAs.

**Our contributions are summarized as:** (i) We introduce a backdoor-theoretic perspective to framework the fundamental principles of AGLAs and identify two critical limitations in their principles: incomplete attack coverage and poor stealthiness. (ii) We propose EGGV to achieve complete attack coverage while evading client-side detection. (iii) Experiments show that EGGV achieves SOTA performance in reconstruction quality, attack coverage, and stealthiness.

## 2. Related Work

### 2.1. Passive Gradient Leakage Attack (PGLA)

Most PGLAs are carried out through gradient matching. DLG (Zhu et al., 2019) is the first attack, which optimizes dummy inputs and labels by matching their gradients to the observed gradients. Its optimization objective is:

$$x'^*, y'^* = \operatorname{argmin}_{x', y'} \left\| \frac{\partial \ell(F(x', \theta), y')}{\partial \theta} - \nabla \theta \right\|^2, \quad (1)$$

Later, iDLG (Zhao et al., 2020) further improves DLG by inferring data labels from the gradients. Subsequent works, such as LLG (Wainakh et al.), extend iDLG to handle larger batch sizes, while other methods (Ma et al., 2023; Wang et al.), such as instance-wise reconstruction (Ma et al., 2023), successfully recover ground-truth labels even in large batches with duplicate labels. IG (Geiping et al., 2020) introduces Total Variation and a Regularization term to im-

prove the optimization objective further. The study (Yin et al., 2021) leverages the mean and variance from batch normalization layers as priors to enhance GLAs. Instead of optimizing dummy inputs directly, GI (Jeon et al., 2021) proposes optimizing the generator and its input latent to generate dummy images whose gradients match the observed gradients. GGL (Li et al., 2022) simplifies this by focusing solely on the latent space of pre-trained BigGAN for gradient matching. More recently, GGDM (Gu et al., 2024) uses captured gradients to guide a diffusion model for reconstruction. However, despite these advancements, PGLAs fail under improper model parameter initializations that yield gradients containing minimal data features. Our experiments in Table 1 and Figure 7, for the first time, question the practical effectiveness of these attacks under popular model initialization methods.

### 2.2. Active Gradient Leakage Attack (AGLA)

Based on the manipulation strategies, most AGLAs can be classified into two categories: structure-modified AGLAs and gradient-biased AGLAs.

**Structure-Modified AGLAs.** This type of attack mainly enhances PGLAs by assuming a dishonest server that manipulates the model structure (Boenisch et al., 2023; Fowl et al., 2021; Nowak et al., 2024; Zhao et al., 2023). Some studies (Fowl et al., 2021; Nowak et al., 2024) insert an FC layer at the beginning of the model, while another work (Zhao et al., 2023) inserts a convolutional layer and two FC layers. These inserted layers are referred to as “trap weights,” which are maliciously modified so that the neurons inside are activated only by samples with specific properties, enabling the reconstruction of the sample with the strongest property. However, modifications to the model structure are inherently detectable due to their explicit changes to the model architecture, rendering them impractical in real-world scenarios. Therefore, this work focuses on another type of AGLAs (Zhang et al., 2022; Wen et al., 2022; Garov et al., 2024) which poisons model parameters instead of modifying the model structure.

**Gradient-Biased AGLAs.** Gradient-biased AGLAs (Zhang et al., 2022; Pasquini et al., 2022; Wen et al., 2022; Garov et al., 2024) poison model parameters to skew the gradient space, ensuring that selected samples dominate the batch-averaged gradients while suppressing others. For instance, Zhang et al. (2022) zero out most of the convolutional layers, ensuring that only one sample’s features reach the classification layer, activating the relevant neurons. Wen et al. (2022) assign many 0s and 1s to the last FC layer to make the averaged gradient close to the gradient of a single sample, thereby enhancing the reconstruction of PGLAs on a single sample. Pasquini et al. (2022) distribute inconsistent models to clients, forcing non-target users’ ReLU layers (Nair &

Hinton, 2010) to output zero gradients, thereby retaining only the target user’s gradients, which can then be exploited to leak the targeted private data. Garov et al. (2024) observe that all these AGLAs bias the averaged gradient toward the gradients of a small subset of data within a batch while suppressing the gradients of other samples. Exploiting this bias in the biased gradients, Garov et al. (2024) introduce a D-SNR detection metric to check poisoned model parameters, which is calculated as below:

$$D - SNR(\theta) = \max_{W \in \theta_{lw}} \frac{\max_{i \in \{1, \dots, B\}} \left\| \frac{\partial \ell(F(x_i), y_i)}{\partial W} \right\|}{\sum_{i=1}^B \left\| \frac{\partial \ell(F(x_i), y_i)}{\partial W} \right\| - \max_{i \in \{1, \dots, B\}} \left\| \frac{\partial \ell(F(x_i), y_i)}{\partial W} \right\|}, \quad (2)$$

where  $\theta_{lw}$  denotes the set of weights of all dense and convolutional layers. D-SNR claims that all prior AGLAs are detectable by principled checks.

### 3. Backdoor-theoretical Analysis

We introduce a new approach for AGLA analysis. It offers a deep insight into the relationship between model parameters and gradient bias, and explains why existing AGLAs are detectable and cannot recover all samples in a batch.

For a simple neural network that is only comprised of fully connected layers  $F(\mathbf{x}) = \mathbf{x}W + \mathbf{b}$ , where  $\mathbf{x} \in \mathbb{R}^{B \times m}$  is a batch of data,  $W \in \mathbb{R}^{m \times n}$  is the weight parameters.  $b \in \mathbb{R}^{1 \times n}$  is the bias, with  $B$  being the batch size and  $n$  being the number of classification categories. When data  $x$  is fed into the model, the output is represented by  $\hat{y} = xW + b$ . As seen in prior work (Fowl et al., 2021), the gradients of the weights and biases of the FC layer can be directly used to reconstruct a weighted average of the input data:

$$\bar{x}^{(k)} = \frac{\nabla_{W^k} \ell(F(x, \theta), y)}{\nabla_{b^k} \ell(F(x, \theta), y)} = \sum_{i=1}^B \lambda_i^k \cdot x_i, \quad (3)$$

where  $k \in [1, n]$  is the class index,  $\nabla_{W^k} \ell(F(x, \theta), y)$  (abbreviated as  $\nabla W^k$ ) denotes the gradient of the  $k^{th}$  column of the weight matrix  $W$ , and  $\nabla_{b^k} \ell(F(x, \theta), y)$  (abbreviated as  $\nabla b^k$ ) represents the gradient of the  $k^{th}$  element of the bias  $b$ .  $\lambda$  is defined as below.

**Theorem 3.1.** *Let  $F(x) = xW + b$  be the classification model with one FC layer, where  $x$  is the input data,  $W$  is the weight matrix, and  $b$  is the bias vector, and the corresponding model output is  $\hat{y} = F(x)$ . Suppose  $\ell(\hat{y}, y)$  is the loss function between the model output  $\hat{y}$  and the ground-truth labels  $y$ . For any class index  $k \in \{1, 2, \dots, n\}$  and sample index  $i \in \{1, 2, \dots, B\}$ , the coefficient  $\lambda$  holds that:*

$$\lambda_i^k = \frac{\frac{\partial \ell(\hat{y}_i^k, y_i)}{\partial \hat{y}_i^k}}{\sum_{j=1}^B \frac{\partial \ell(\hat{y}_j^k, y_j)}{\partial \hat{y}_j^k}}, \text{ and } \sum_{i=1}^B \lambda_i^k = 1, \quad (4)$$

where  $\partial \ell(\hat{y}_i^k, y_i) / \partial \hat{y}_i^k$  denotes the partial derivative of the loss function with respect to the output  $\hat{y}_i^k$ .

*Proof.* See our proof in Appendix B.1.  $\square$

Taking a binary classification network with an input of 4 samples as an example, the weighted average sample obtained by the gradient of the weights and biases of the two categories can be expressed as:

$$\begin{bmatrix} \frac{\nabla W^1}{\nabla b^1} \\ \frac{\nabla W^2}{\nabla b^2} \end{bmatrix} = \begin{bmatrix} \bar{x}^{(1)} \\ \bar{x}^{(2)} \end{bmatrix} = \begin{bmatrix} \lambda_1^1 & \lambda_2^1 & \lambda_3^1 & \lambda_4^1 \\ \lambda_1^2 & \lambda_2^2 & \lambda_3^2 & \lambda_4^2 \end{bmatrix} \begin{bmatrix} x_1 \\ x_2 \\ x_3 \\ x_4 \end{bmatrix} = \Lambda \mathbf{X}. \quad (5)$$

Equation (5) shows the weighted average data resolved by the gradient of the weights and biases *w.r.t* a given class, which is actually a weighted summation of the features of the input layer.  $\lambda$  is exactly the weight factor to quantify the bias in the gradient space of neurons toward specific samples within a batch.

$\lambda$  is crucial for the gradient-biased AGLAs, as it controls the weighted feature proportions computed from gradients. It is the first technical measure to quantify the relative contribution of each sample in the batch to the activation of each class of neurons in the model. Interestingly, we find the AGLAs are very analogous to poisoning-based backdoor attacks. In the later, the attacker poisons the model training process to an expected state to manipulate the model output and eventually control the distribution of  $\lambda$ . Therefore, we call this approach the backdoor-theoretical perspective.

The core mechanism of manipulating  $\lambda$  inherently introduces several challenges: (1) samples without gradient space bias cannot be reconstructed; (2) reconstruction becomes impossible when two samples with the required properties coexist; and (3) the presence of anomalous gradients in the gradient space makes the attack detectable. This explains the fundamental limitations of existing AGLAs.

### 4. Enhanced Gradient Global Vulnerability

The above-mentioned challenges suggest that instead of controlling  $\lambda$  to achieve reconstruction, we should focus on increasing the concentration of input features and enhancing feature representation at the source rather than compressing the features of some samples to amplify others. Following this inspiration, we introduce EGGV, a new attack that poisons the model parameters  $\theta$  to equally enhance the leakage potential of all samples in a batch, thus ensuring a comprehensive attack and evading detection. Figure 2 provides an intuitive comparison between EGGV and existing Gradient-biased AGLAs. While existing attacks achieve reconstruction by suppressing the features of non-target samples to amplify those of specific ones in gradient, EGGV instead uniformly enhances the encoded features of each samples in gradient, following an entirely different principle.

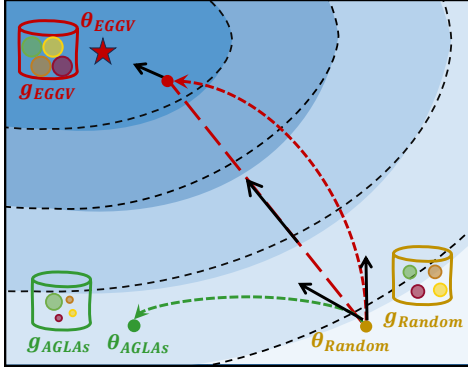


Figure 2. Fundamental principle comparison between EGGV and gradient-biased AGLAs.

#### 4.1. Threat Model

Our threat model operates within a federated learning (FL) framework where the server is dishonest and curious. It manipulates the model parameters before distributing them to clients but is restricted from altering the model structure. By exploiting this capability, the server poisons the model parameters to amplify the gradient vulnerabilities, thereby enabling the reconstruction of clients’ data from the uploaded gradients. Furthermore, we assume the malicious client has access to publicly available datasets, which can be used as auxiliary data to facilitate the attack.

#### 4.2. Attack Overview

The proposed EGGV is comprised of three main steps. Algorithm 1 in Appendix A shows the detailed process. Figure 3 provides a visual overview of EGGV.

**Step I:** The malicious server poisons the global model before its distribution (Step ① in Figure 3, `PoisonModel` in Algorithm 1). In this stage, the server iteratively optimizes the global model and discriminator locally with the objective function  $L(\theta, \phi)$  using an auxiliary dataset, enriching the gradients with encoded features.

**Step II:** The server distributes the poisoned model to clients (Step ② in Figure 3, `CollectClientGradients` in Algorithm 1). Each client, following the FL protocol, feeds its own training data into the poisoned model to generate gradients that are then uploaded back to the server.

**Step III:** The server uses these uploaded gradients to perform data reconstruction using any existing PGLAs (Step ③ in Figure 3, `ReconstructData` in Algorithm 1).

#### 4.3. Problem Formulation

The objective of the malicious server is to minimize the difference between the reconstructed data and the original data. Formally, we have the following objective:

$$\theta^* = \operatorname{argmin}_{\theta} \|x - x'\|_p, \quad (6)$$

where  $x$  represents one data batch from the auxiliary dataset  $D$ , and  $x'$  denotes the reconstructed data obtained by the attacker using the gradient leakage method  $R(\cdot)$ . These gradients are computed on the client side during local training. Specifically, the client inputs local training data  $x$  into the model, yielding the output  $\hat{y} = F(x, \theta)$ , and then calculates the gradient  $\frac{\partial \ell(F(x, \theta), y)}{\partial \theta}$ . The optimization objective can therefore be expanded as follows:

$$\theta^* = \operatorname{argmin}_{\theta} \|x - R\left(\frac{\partial \ell(F(x, \theta), y)}{\partial \theta}\right)\|_p. \quad (7)$$

The server aims to optimize the model parameters  $\theta$  such that the reconstructed data obtained via the gradient leakage method  $R(\cdot)$ , closely approaches the original input data  $x$ .

#### 4.4. Detailed Solution

As shown in Equation (7), the performance of the gradient leakage attack depends on the model parameters, meaning there exists an optimal set of model parameters, denoted as  $\theta^*$ , that minimizes the reconstruction loss between the original data  $x$  and the recovered data  $x'$  given a specific reconstruction function  $R(\cdot)$ .

To search in the continuous parameter space for the optimal model parameters, we introduce a dimension reduction projector  $\Pi(\cdot)$ . Specifically, for a data batch  $x$ , the gradients  $g = \nabla_{\theta} \ell(F(x, \theta), y)$  on the global model are sampled by the projector  $\Pi(\cdot)$  at fixed positions, ensuring that the gradients have consistent positions during the iterations:

$$\Pi(g) = (g_1[p_1], \dots, g_L[p_L], \rho)^T, \quad (8)$$

where  $p_1, \dots, p_L$  represent pre-specified sets of gradient positions from the 1<sup>st</sup> to the  $L^{\text{th}}$  layer, indicating the fixed positions of the gradients sampled during each iteration.  $\rho$  represents the ratio of the number of parameters of the projected gradient to that of the original gradient, and we hereinafter refer to it as the projection ratio. By applying the projector  $\Pi(\cdot)$ , we map the high-dimensional gradient space into a lower-dimensional vector space as follows:

$$\tilde{g} = \Pi\left(\frac{\partial \ell(F(x, \theta), y)}{\partial \theta}\right). \quad (9)$$

With the projected gradient, we introduce a discriminator  $\mathcal{D}(\cdot)$  to evaluate the potential for gradient leakage by the projected gradient. Equation (7) measures the vulnerability of the corresponding gradient space by performing an end-to-end reconstruction attack and computes the similarity between the reconstructed and original data. Traditional end-to-end reconstruction attacks require performing gradient matching in Equation (1) and then optimizing on dummy data. This method has a high computational cost, as it requires iterative operations in the continuous gradient space

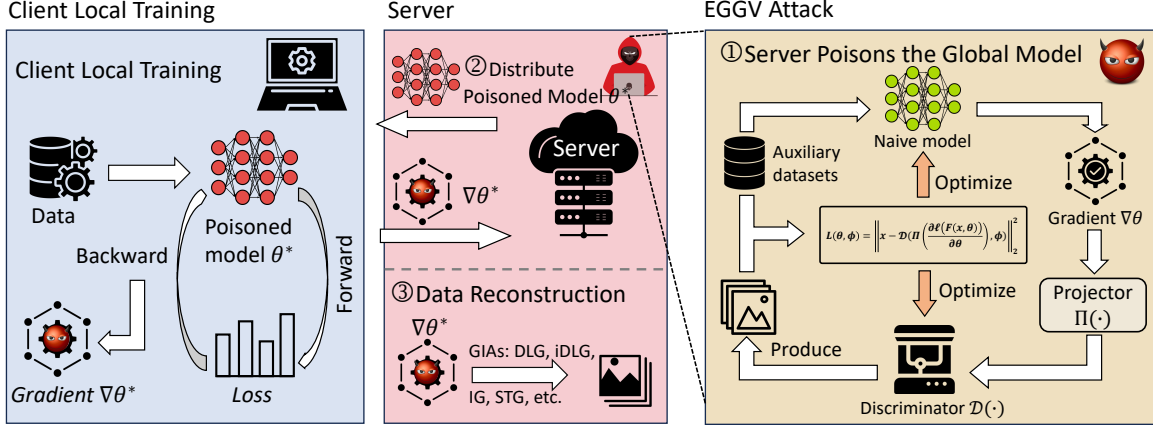


Figure 3. Overview of the proposed EGGV, consisting of three steps: ① poison the model parameters to make its gradient space vulnerable; ② distribute poisoned model and gather vulnerable gradients; ③ implement existing GLAs on these gradients.

for each update of  $\theta$ . Additionally, iterative reconstruction introduces a nested optimization structure, making it challenging to compute the second-order derivative of the loss.

Prior GLAs suggest that the gradient vulnerability stems from the data features they encode. The more data features a gradient contains, the more vulnerable that gradient becomes. To this end, *the gradients can be encoded representations of input data*, while the forward and backward propagation within the model is the encoding process.

The goal of the proposed EGGV is to refine this encoding process to maximize the retention of input data features within the gradients. To achieve this, we design a decoder that decodes the projected gradients to the original input. The attacker jointly optimizes the model and the decoder by the following loss function:

$$L(\theta, \phi) = \left\| x - \mathcal{D} \left( \Pi \left( \frac{\partial \ell(F(x, \theta), y)}{\partial \theta} \right), \phi \right) \right\|_2^2, \quad (10)$$

where  $\phi$  represents the parameters of the decoder  $\mathcal{D}$ .

#### 4.5. Optimal Model for the Gradient Leakage

We prove a global minimum exists for the proposed loss function, where the corresponding model parameters maximize the vulnerability of gradient space to data leakage.

**Assumption 4.1.** The global model  $F(\theta)$  is continuous, and the parameter space  $\Theta$  of  $\theta$  is a non-empty compact set.

**Assumption 4.2.** The loss function  $\ell(\cdot, \cdot)$  for the client training is continuously differentiable with respect to the model parameters  $\theta$ , allowing for gradient computation with respect to  $\theta$ .

**Assumption 4.3.** The decoder  $\mathcal{D}$  is a linear function of the form  $\mathcal{D}(\tilde{g}) = W \cdot \tilde{g} + b$  and is continuous. The parameter space  $\Phi$  of  $\phi$  is a non-empty compact set.

**Theorem 4.1.** *Under the above assumptions, there exists parameters  $\theta^* \in \Theta$ ,  $\phi^* \in \Phi$  such that the loss function*

$L(\theta, \phi)$  defined in Equation (10) attains its global minimum:

$$\theta^*, \phi^* = \arg \min_{\theta \in \Theta, \phi \in \Phi} L(\theta, \phi). \quad (11)$$

At  $\theta = \theta^*$ ,  $\phi = \phi^*$ , the gradient  $\nabla_{\theta} \ell(F(x, \theta), y)$  encodes the maximum amount of feature from the input data  $x$ , making the gradient space most susceptible to leakage.

*Proof.* The proof is in Appendix B.2.  $\square$

## 5. Experimental Evaluation

In this section, we present a series of experiments to evaluate the effectiveness of the proposed method. The experiment results show that EGGV significantly outperforms the SOTA AGLAs in reconstruction quality and stealthiness.

### 5.1. Setup

We use the ResNet18 (He et al., 2016) as the default global model for FL. The CIFAR10, CIFAR100 (Krizhevsky et al., 2009), and TinyImageNet (Le & Yang, 2015) datasets are employed as the training data for clients. Following (Garov et al., 2024), we generally use the training set as auxiliary data and implement an attack on randomly sampled batches of size  $B$  from the test set. The three classic evaluation metrics for reconstruction quality, namely PSNR (Hore & Ziou, 2010), SSIM (Zhang et al., 2018), and LPIPS (Wang et al., 2004), are employed to assess the attack quality. We use the detection metric D-SNR (Garov et al., 2024) to evaluate the stealthiness of model modifications. We set the default projection ratio to 0.4% and employ a linear layer as the default structure for the discriminator. We compare our method with the closely related SOTA methods, Fishing (Wen et al., 2022) and SEER (Garov et al., 2024) with the maximal brightness as the selected property. As our method is the first to poison model parameters for enhanced data leakage across entire batches, we also evaluate its performance

Table 1. Performance comparison of the proposed EGGV against baseline model initializations Random, Xavier, and He on CIFAR10, CIFAR100, and TinyImageNet datasets.

Method	CIFAR10			CIFAR100			TinyImageNet		
	PSNR $\uparrow$	SSIM $\uparrow$	LPIPS $\downarrow$	PSNR $\uparrow$	SSIM $\uparrow$	LPIPS $\downarrow$	PSNR $\uparrow$	SSIM $\uparrow$	LPIPS $\downarrow$
Random+iDLG	15.8685	0.5955	0.2896	16.9960	0.5372	0.3441	14.0472	0.2229	0.5755
Xavier+iDLG	20.7717	0.7864	0.2469	19.8529	0.7310	0.2683	12.1854	0.2305	0.5859
He+iDLG	-1.1551	-0.0005	0.7238	-1.9460	-0.0017	0.7527	-1.0535	-0.0004	0.8001
EGGV(Ours)+iDLG	<b>29.7010</b>	<b>0.8649</b>	<b>0.1081</b>	<b>28.4425</b>	<b>0.8970</b>	<b>0.0906</b>	<b>19.9437</b>	<b>0.6267</b>	<b>0.2210</b>
Random+IG	19.1621	0.6219	0.3076	19.3464	0.6383	0.3140	15.4700	0.2563	0.5208
Xavier+IG	24.4702	0.8633	0.1444	23.1615	0.8044	0.1723	13.0624	0.2185	0.5737
He+IG	13.3073	0.1019	0.6242	10.9789	0.0907	0.6628	12.7034	0.2088	0.7256
EGGV(Ours)+IG	<b>31.9651</b>	<b>0.9166</b>	<b>0.0735</b>	<b>31.5515</b>	<b>0.9267</b>	<b>0.0617</b>	<b>28.6232</b>	<b>0.9140</b>	<b>0.0757</b>

Table 2. Comparison of reconstruction performance among EGGV (Ours), Fishing (Wen et al., 2022), and SEER (Garov et al., 2024) on CIFAR100 with a batch size of 8.

	Min PSNR $\uparrow$	Pruned Average PSNR $\uparrow$	Max PSNR $\uparrow$
Fishing (Wen et al., 2022)	0.00000	0.00000	12.92526
SEER (Garov et al., 2024)	0.00000	0.00000	15.97548
EGGV (Ours)	<b>20.37788</b>	<b>21.59001</b>	<b>22.86605</b>

against popular naive model initialization methods, including Random, Xavier (Glorot & Bengio, 2010), and He (He et al., 2015). In our implementation, Xavier initialization uses a uniform distribution to balance variance across layers, while He initialization adapts weights for leaky ReLU activations, to ensure smoother gradient flow during training. We also provide more results in the Appendix C.

## 5.2. Main Results

**Comparison between EGGV and SOTA AGLAs.** Firstly, we compare the performance of the proposed EGGV with two SOTA AGLAs, Fishing (Wen et al., 2022), and SEER (Garov et al., 2024), on CIFAR100 with a batch size of 8. Table 2 reports the minimum PSNR, pruned average PSNR, and maximum PSNR over 100 batches, where a PSNR of 0 indicates no reconstruction. EGGV achieves significantly higher PSNR, consistently reconstructing all samples per batch with minimal variation, while SOTA methods reconstruct only one sample per batch. We also provide a visual comparison of reconstruction results in Figure 7.

**Comparison between EGGV and Popular Model Initialization Methods in Enhancing PGLAs.** Considering that EGGV is the first AGLA to reconstruct all samples in the batch, we compare its performance with three naive model initialization methods. We implement the iDLG (Zhao et al., 2020) and IG (Geiping et al., 2020) on models that proposed EGGV poisons, naively initialized by Random, Xavier, and He. As shown in Table 1 the EGGV significantly outperforms Random, Xavier, and He initialization methods across all three datasets, regardless of whether iDLG or IG is used.

Figure 7 provides a visual comparison of reconstruction results, clearly illustrating the superiority of EGGV.

He initialization is widely recognized for its advantages in global model training when used by honest servers, but it often results in attack failures for adversaries, including the server itself. This indicates that relying solely on original model parameters results in poor attack performance. Our research further shows that to improve the effectiveness of attacks, adversaries cannot rely only on standard model parameters. Instead, they should adopt poisoning techniques like EGGV to actively manipulate the gradient space.

The experimental results also highlight the critical importance of the gradient position within the gradient space for the success of GLAs. Unfortunately, previous PGLAs have overlooked this factor. Traditional PGLAs are typically limited by the current state of the model parameters, thus making it difficult to achieve optimal results. Although AGLAs attempt to address this by poisoning model parameters, their effectiveness is limited to a small subset of samples within the batch, as illustrated in Figure 7. Notably, EGGV is the first method to tackle this key challenge for both PGLAs and AGLAs by poisoning model parameters to enhance the gradient vulnerability across the entire batch.

**Stealthiness Comparisons of EGGV with SOTA AGLAs.** We calculate 100 gradients on CIFAR100 with each ResNet18 poisoned by Fishing, SEER, and EGGV and initialized by naive initialization methods Random, Xavier, and He. We then report the D-SNR values for these gradients. As illustrated in Figure 5, EGGV demonstrates high stealthiness, achieving D-SNR values similar to those of the naive initialization methods Random, Xavier, and He. In contrast, Fishing and SEER show significantly higher D-SNR values, suggesting that clients can detect these methods more easily. This is because EGGV evenly enhances the leakage potential of all samples without introducing any gradient bias. In contrast, SOTA methods exhibit biased gradients across all layers, making them more prone to detection.

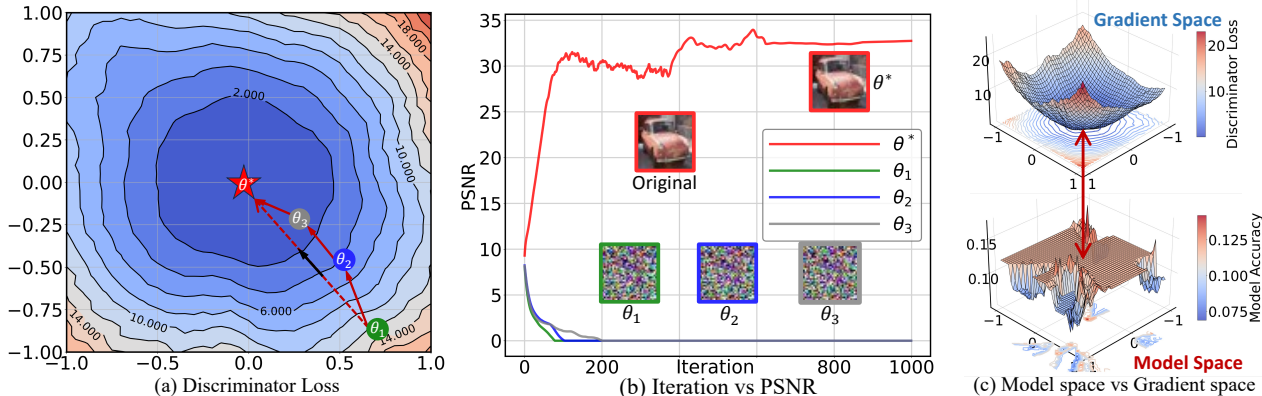


Figure 4. Figure (a): Contour map of the discriminator loss landscape across 441 model parameters generated by shifting  $\theta^*$  along two random directions. The map marks the selected points  $\theta_1$ ,  $\theta_2$ ,  $\theta_3$ , and  $\theta^*$ . Figure (b): PSNR curves from IG attacks on a ResNet18 model at  $\theta_1$ ,  $\theta_2$ ,  $\theta_3$ , and  $\theta^*$ , demonstrating that  $\theta^*$  achieves the best reconstruction quality. Figure (c): 3D surface plots of the discriminator loss (top) and model accuracy (bottom) for the same 441 model parameters shifted  $\theta^*$  along two random directions, illustrating the relationship between gradient vulnerability and model accuracy across the parameters space.

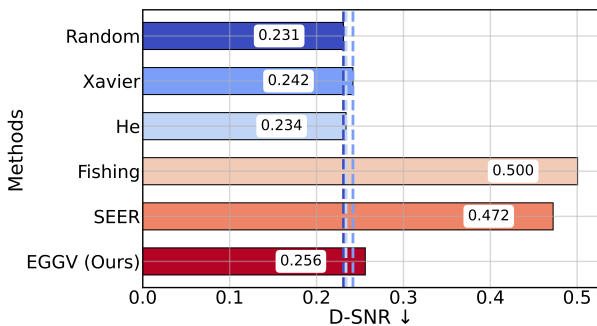


Figure 5. Bar chart of D-SNR value of gradients generated by models with three naive initialization methods (Random, Xavier, He) and three poisoning methods (Fishing, SEER, EGGV) on 100 same batches. Lower values indicate greater stealthiness. EGGV achieves a highly stealthy, closely approaching D-SNR of standard initialization methods.

### 5.3. Ablation Experiment

**Evaluating Gradient Space Vulnerability Using the Discriminator Instead of End-to-End Iterative Attacks.** We now turn to explore the effectiveness of using a discriminator to assess gradient space vulnerability, as opposed to traditional end-to-end iterative attacks. We randomly select two model directions,  $x$  and  $y$ , in the model parameters space and systematically shift the poisoned model parameter  $\theta^*$  along these axes, generating 441 model parameters. The discriminator evaluates the gradient vulnerability for each of these parameters, and the resulting contour map of gradient vulnerability is shown in Figure 4(a). In this map, we select four points:  $\theta_1$ ,  $\theta_2$ ,  $\theta_3$ ,  $\theta^*$ , with corresponding vulnerability scores of 14.99276, 5.42985, 1.28999, and 0.00655 assigned by the discriminator. Subsequently, we perform the IG attack on these four models with the CIFAR10 dataset. Figure 4(b) depicts the PSNR convergence during the attacks on these four models. As expected,  $\theta^*$  yields the best reconstruction. The reconstructed images are highly simi-

lar to the original input, and the PSNR value remains the highest throughout the convergence process, significantly outperforming the other three parameters. These findings demonstrate the discriminator’s effectiveness in evaluating gradient space vulnerability and predicting the likelihood of a successful reconstruction attack. In contrast to traditional end-to-end reconstruction methods, this method enables attackers to quickly identify and poison model parameters that could lead to attack failure, thereby improving the overall success rate for attacks.

**Exploring the Relationship Between Gradient Space Vulnerability and Model Accuracy.** To explore the relationship between gradient vulnerability and model accuracy, we conduct experiments by shifting the poisoned model parameter  $\theta^*$  evenly 21 times along two randomly selected directions,  $x$  and  $y$ , generating 441 model parameters. Each parameter receives a gradient vulnerability score from the discriminator, visualized in the 3D surface plot at the top of Figure 4(c), representing the gradient vulnerability landscape across the parameters space. We then evaluate the classification accuracy of these same 441 model parameters using the CIFAR10 dataset, producing the lower plot of Figure 4(c). This plot shows the model accuracy at the same parameter positions as in the gradient vulnerability plot. A comparison between the two plots reveals that the model parameters with the highest gradient vulnerability do not coincide with those that yield the highest accuracy. In fact, model parameters with the greatest gradient vulnerability often show low accuracy, indicating no direct correlation between gradient vulnerability and model accuracy.

**The Effect of Different Gradient Projection Ratios.** A crucial component of the EGGV is the projector, which compresses high-dimensional gradients into a one-dimensional vector. Next, we examine how different projection ratios influence EGGV to enhance the vulnerability of the gradi-

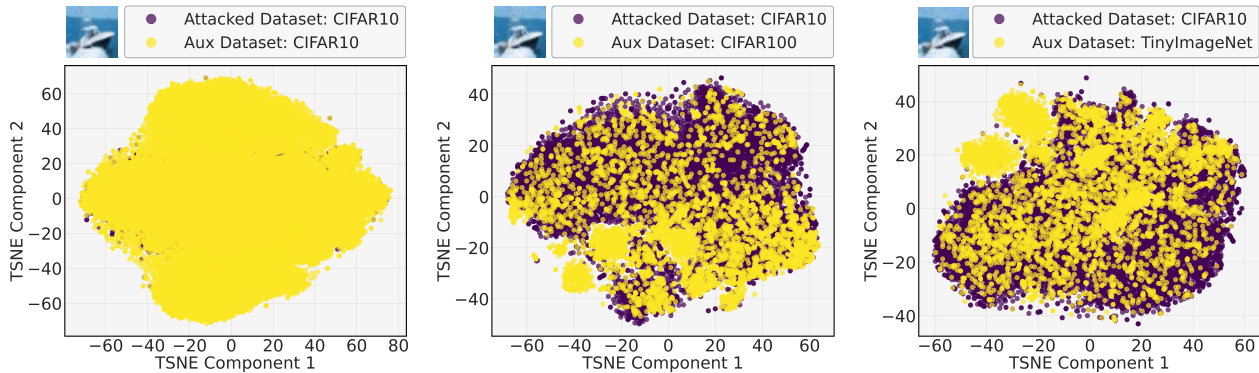


Figure 6. Visualization of distributional differences between auxiliary and target datasets and IG reconstruction results on EGGV-poisoned models using each auxiliary dataset.

Table 3. Reconstruction results of IG attack ResNet18 poisoned by EGGV with projection ratios of 1.60%, 0.80%, and 0.40%. EGGV at 0.40% projection ratio achieves the best overall performance.

Initiation Method	PSNR $\uparrow$	SSIM $\uparrow$	LPIPS $\downarrow$
Random	15.4700	0.2563	0.5208
EGGV (Ours) ( $\rho$ : 1.60%) + IG	25.2461	0.8065	0.1280
EGGV (Ours) ( $\rho$ : 0.80%) + IG	27.6307	0.8575	0.0952
EGGV (Ours) ( $\rho$ : 0.40%) + IG	<b>28.6232</b>	<b>0.9140</b>	<b>0.0757</b>

ent space. We select commonly used Random initialization methods as comparison benchmarks, and set three different gradient projection ratios of 1.60%, 0.80%, and 0.40%. IG is used to conduct gradient leakage on the TinyImageNet dataset with the models initialized by the Random and EGGV. Comparison experimental results in Table 3 show that EGGV consistently enhances the gradient vulnerability across all three projection ratios, outperforming Random initialization methods. We observe an interesting phenomenon: the smallest projection ratio of 0.4% achieves the best effect. This phenomenon can be attributed to the fact that smaller projection ratios force the model to embed more data features into the entire gradient, ensuring that the projected gradients retain enough data features to be inverted by the discriminator back to the original input. Under a smaller projection ratio, the model will more actively adjust its own parameters, thus containing more data features in the entire gradient, which is more conducive to the attack of subsequent attack methods.

**Exploring the Effect of Distribution Differences Between Auxiliary and Target Datasets on EGGV.** Next, we explore the effect of distributional differences between auxiliary and target datasets on the performance of the EGGV. We select CIFAR10 as the target dataset and CIFAR10, CIFAR100, and TinyImageNet as the auxiliary datasets. To align the class counts with CIFAR10 to ensure compatibility for model poisoning, 10 classes are randomly sampled from CIFAR100 and TinyImageNet to serve as auxiliary datasets. Table 4 reports the performance of iDLG and IG attacks on EGGV-poisoned models with the CIFAR10 test set as the target dataset, using different auxiliary datasets. The results

Table 4. Performance of iDLG and IG attacks on EGGV-poisoned models using different auxiliary datasets with CIFAR10 as the target dataset. EGGV achieves comparable PSNR values across all auxiliary datasets, demonstrating its robustness to distributional differences between auxiliary and target datasets.

Attacked Dataset:	Auxiliary Datasets (PSNR $\uparrow$ )		
	CIFAR10	CIFAR100	TinyImageNet
EGGV+iDLG	29.70104	29.93789	31.83867
EGGV+IG	31.96511	31.28306	31.64095

show that EGGV achieves comparable PSNR values across CIFAR10, CIFAR100, and TinyImageNet auxiliary datasets, highlighting its robustness to distributional differences between auxiliary and target datasets. In addition, we use the t-SNE algorithm (Van der Maaten & Hinton, 2008) to reduce the dimensionality of these datasets to 2D and visualize the data distribution of the auxiliary and target datasets, along with the corresponding reconstruction results shown in Figure 6. The visualizations confirm that the effectiveness of the EGGV attack is independent of distributional differences between the auxiliary and target datasets. In contrast, some SOTA methods such as SEER require the auxiliary dataset to be the training data set of the target dataset, which limits their application to practical FL systems.

## 6. Conclusion

In this work, we introduce a new backdoor-theoretic perspective to rethink and framework existing AGLAs. Through this lens, we identify that all prior AGLAs suffer from incomplete attack coverage and detectability issues. We further propose EGGV, a new solution that extends existing AGLAs to be more comprehensive and stealthier to address above challenges. EGGV is the first AGLA capable of fully inverting all samples within a target batch while evading existing detection metrics. Extensive experiments demonstrate that EGGV significantly outperforms SOTA AGLAs in both stealthiness and attack coverage. These results encourage the FL community to explore further privacy protection mechanisms to counter these emerging security risks.



## Impact Statement

We believe that the proposed theoretical analysis approach and novel attack are beneficial to the FL community. Our efforts are not to undermine the overall security of FL but rather to present new potential risks brought by gradients shared in the FL framework. We hope that our insights will spark further exploration of robust defense mechanisms against privacy breaches in FL systems, thereby strengthening the trustworthiness and resilience of these increasingly important collaborative learning frameworks.

## References

- Bartle, R. and Sherbert, D. *Introduction to Real Analysis*. Wiley, 2011. ISBN 9781118135860. URL <https://books.google.com.sg/books?id=YawbAAAAQBAJ>.
- Boenisch, F., Dziedzic, A., Schuster, R., Shamsabadi, A. S., Shumailov, I., and Papernot, N. When the curious abandon honesty: Federated learning is not private. In *2023 IEEE 8th European Symposium on Security and Privacy (EuroS&P)*, pp. 175–199. IEEE Computer Society, 2023.
- Bonawitz, K. A., Eichner, H., Grieskamp, W., Huba, D., Ingerman, A., Ivanov, V., Kiddon, C. M., Konečný, J., Mazzocchi, S., McMahan, B., Overveldt, T. V., Petrou, D., Ramage, D., and Roselander, J. Towards federated learning at scale: System design. In *SysML 2019*, 2019. URL <https://arxiv.org/abs/1902.01046>. To appear.
- Chilimbi, T., Suzue, Y., Apacible, J., and Kalyanaraman, K. Project adam: Building an efficient and scalable deep learning training system. In *11th USENIX symposium on operating systems design and implementation (OSDI 14)*, pp. 571–582, 2014.
- Fowl, L. H., Geiping, J., Czaja, W., Goldblum, M., and Goldstein, T. Robbing the fed: Directly obtaining private data in federated learning with modified models. In *International Conference on Learning Representations*, 2021.
- Garov, K., Dimitrov, D. I., Jovanović, N., and Vechev, M. Hiding in plain sight: Disguising data stealing attacks in federated learning. In *International Conference on Learning Representations*, 2024.
- Geiping, J., Bauermeister, H., Dröge, H., and Moeller, M. Inverting gradients-how easy is it to break privacy in federated learning? *Advances in neural information processing systems*, 33:16937–16947, 2020.
- Glorot, X. and Bengio, Y. Understanding the difficulty of training deep feedforward neural networks. In *Proceedings of the thirteenth international conference on artificial intelligence and statistics*, pp. 249–256. JMLR Workshop and Conference Proceedings, 2010.
- Gu, H., Zhang, X., Li, J., Wei, H., Li, B., and Huang, X. Federated learning vulnerabilities: Privacy attacks with denoising diffusion probabilistic models. In *Proceedings of the ACM on Web Conference 2024*, pp. 1149–1157, 2024.
- He, K., Zhang, X., Ren, S., and Sun, J. Delving deep into rectifiers: Surpassing human-level performance on imagenet classification. In *Proceedings of the IEEE international conference on computer vision*, pp. 1026–1034, 2015.
- He, K., Zhang, X., Ren, S., and Sun, J. Deep residual learning for image recognition. In *Proceedings of the IEEE conference on computer vision and pattern recognition*, pp. 770–778, 2016.
- Hore, A. and Ziou, D. Image quality metrics: Psnr vs. ssim. In *2010 20th international conference on pattern recognition*, pp. 2366–2369. IEEE, 2010.
- Jeon, J., Lee, K., Oh, S., Ok, J., et al. Gradient inversion with generative image prior. *Advances in neural information processing systems*, 34:29898–29908, 2021.
- Krizhevsky, A., Hinton, G., et al. Learning multiple layers of features from tiny images. 2009.
- Le, Y. and Yang, X. Tiny imagenet visual recognition challenge. *CS 231N*, 7(7):3, 2015.
- Li, Z., Zhang, J., Liu, L., and Liu, J. Auditing privacy defenses in federated learning via generative gradient leakage. In *Proceedings of the IEEE/CVF Conference on Computer Vision and Pattern Recognition*, pp. 10132–10142, 2022.
- Ma, K., Sun, Y., Cui, J., Li, D., Guan, Z., and Liu, J. Instance-wise batch label restoration via gradients in federated learning. In *The Eleventh International Conference on Learning Representations*, 2023.
- McMahan, B., Moore, E., Ramage, D., Hampson, S., and y Arcas, B. A. Communication-efficient learning of deep networks from decentralized data. In *Artificial intelligence and statistics*, pp. 1273–1282. PMLR, 2017.
- Nair, V. and Hinton, G. E. Rectified linear units improve restricted boltzmann machines. In *Proceedings of the 27th international conference on machine learning (ICML-10)*, pp. 807–814, 2010.
- Nowak, M. V., Bott, T. P., Khachaturov, D., Puppe, F., Krenzer, A., and Hekalo, A. Qbi: Quantile-based bias initialization for efficient private data reconstruction in federated learning. *arXiv preprint arXiv:2406.18745*, 2024.

- Pasquini, D., Francati, D., and Ateniese, G. Eluding secure aggregation in federated learning via model inconsistency. In *Proceedings of the 2022 ACM SIGSAC Conference on Computer and Communications Security*, pp. 2429–2443, 2022.
- Rudin, W. *Principles of Mathematical Analysis*. International series in pure and applied mathematics. McGraw-Hill, 1976. ISBN 9780070856134. URL <https://books.google.com.sg/books?id=kwqzPAAACAAJ>.
- Van der Maaten, L. and Hinton, G. Visualizing data using t-sne. *Journal of machine learning research*, 9(11), 2008.
- Wainakh, A., Ventola, F., Müßig, T., Keim, J., Cordero, C. G., Zimmer, E., Grube, T., Kersting, K., and Mühlhäuser, M. User-level label leakage from gradients in federated learning. *Proceedings on Privacy Enhancing Technologies*, 2022(2):227–244.
- Wang, Y., Liang, J., and He, R. Towards eliminating hard label constraints in gradient inversion attacks. In *The Twelfth International Conference on Learning Representations*.
- Wang, Z., Bovik, A. C., Sheikh, H. R., and Simoncelli, E. P. Image quality assessment: from error visibility to structural similarity. *IEEE transactions on image processing*, 13(4):600–612, 2004.
- Wen, Y., Geiping, J. A., Fowl, L., Goldblum, M., and Goldstein, T. Fishing for user data in large-batch federated learning via gradient magnification. In *International Conference on Machine Learning*, pp. 23668–23684. PMLR, 2022.
- Yang, H., Ge, M., Xiang, K., and Li, J. Using highly compressed gradients in federated learning for data reconstruction attacks. *IEEE Transactions on Information Forensics and Security*, 18:818–830, 2022.
- Yin, H., Mallya, A., Vahdat, A., Alvarez, J. M., Kautz, J., and Molchanov, P. See through gradients: Image batch recovery via gradinversion. In *Proceedings of the IEEE/CVF conference on computer vision and pattern recognition*, pp. 16337–16346, 2021.
- Yue, K., Jin, R., Wong, C.-W., Baron, D., and Dai, H. Gradient obfuscation gives a false sense of security in federated learning. In *32nd USENIX Security Symposium (USENIX Security 23)*, pp. 6381–6398, Anaheim, CA, August 2023. USENIX Association. ISBN 978-1-939133-37-3. URL <https://www.usenix.org/conference/usenixsecurity23/presentation/yue>.
- Zhang, R., Isola, P., Efros, A. A., Shechtman, E., and Wang, O. The unreasonable effectiveness of deep features as a perceptual metric. In *Proceedings of the IEEE conference on computer vision and pattern recognition*, pp. 586–595, 2018.
- Zhang, S., Huang, J., Zhang, Z., and Qi, C. Compromise privacy in large-batch federated learning via malicious model parameters. In *International Conference on Algorithms and Architectures for Parallel Processing*, pp. 63–80. Springer, 2022.
- Zhao, B., Mopuri, K. R., and Bilen, H. idlg: Improved deep leakage from gradients. *arXiv preprint arXiv:2001.02610*, 2020.
- Zhao, J. C., Sharma, A., Elkordy, A. R., Ezzeldin, Y. H., Avestimehr, S., and Bagchi, S. Loki: Large-scale data reconstruction attack against federated learning through model manipulation. In *2024 IEEE Symposium on Security and Privacy (SP)*, pp. 30–30. IEEE Computer Society, 2023.
- Zhu, J. and Blaschko, M. B. R-gap: Recursive gradient attack on privacy. In *International Conference on Learning Representations*, 2021.
- Zhu, L., Liu, Z., and Han, S. Deep leakage from gradients. *Advances in neural information processing systems*, 32, 2019.

## A. Algorithm for EGGV

---

### Algorithm 1 Poisoning and Reconstruction of EGGV

---

```

1: Input: Auxiliary dataset  $D_a$ , global model  $F(\theta)$ , acceptable error  $\epsilon$ , number of iterations  $N$ 
2: Output: Reconstructed data  $x'$ 
3: Main Process:
4:  $F(\theta^*) \leftarrow \text{PoisonModel}(D_a, F(\theta), N)$ 
5:  $\nabla\theta^* \leftarrow \text{CollectClientGradients}(F(\theta^*))$ 
6:  $x' \leftarrow \text{ReconstructData}(\nabla\theta^*)$ 
7: return  $x'$ 
8: function POISONMODEL( $D_a, F(\theta), N$ )
9:   Initialize  $\theta_0$  randomly
10:   $t \leftarrow 0$ 
11:  while  $L(\theta_t, \phi_t) < \epsilon$  do
12:    for each  $(x_j, y_j) \in D_a$  do
13:       $L(\theta_t, \phi_t) \leftarrow \left\| x_j - \mathcal{D} \left( \Pi \left( \frac{\partial \ell(F(x_j, \theta_t), y_j)}{\partial \theta_t} \right), \phi_t \right) \right\|_2^2$ 
14:      Update  $\theta_t, \phi_t$  using gradient descent:
15:       $\theta_{t+1} \leftarrow \theta_t - \alpha_1 \nabla_{\theta_t} L(\theta_t, \phi_t)$ 
16:       $\phi_{t+1} \leftarrow \phi_t - \alpha_2 \nabla_{\phi_t} L(\theta_t, \phi_t)$ 
17:       $t \leftarrow t + 1$ 
18:    end for
19:  end while
20:  return  $F(\theta^*)$  with updated  $\theta$ 
21: end function
22: function COLLECTCLIENTGRADIENTS( $F(\theta^*)$ )
23:  Client  $i$  receives the global model  $F(\theta^*)$ 
24:  Client  $i$  calculates the gradient  $\nabla_{\theta^*} \ell(F(x, \theta^*), y)$  using its data  $(x, y)$ 
25:  return  $\nabla_{\theta^*} \ell(F(x, \theta^*), y)$ 
26: end function
27: function RECONSTRUCTDATA( $\nabla\theta^*$ )
28:  Select any prior PGLA methods  $R(\cdot)$ 
29:  Reconstruct client data  $x'$  through  $R(\nabla\theta^*)$ 
30:  return reconstructed data  $x'$ 
31: end function

```

---

## B. Proof

### B.1. Proof for Theorem 3.1

*Proof.* Consider a batch of  $B$  samples  $\{(x_i, y_i)\}_{i=1}^B$ , where  $x \in \mathbb{R}^{B \times \text{Channel} \times \text{Height} \times \text{Width}}$  represents the input data and  $y_i$  are the corresponding ground-truth labels. The model outputs for each sample within a batch are given by:  $\hat{y}_i = x_i W + b \in \mathbb{R}^C$ . The total loss over the batch is  $\frac{1}{B} \sum_{i=1}^B \ell(\hat{y}_i, y_i)$ . Next, we derive the gradients of weights and biases for the  $k^{\text{th}}$  class and express the ratio  $\frac{\nabla W^k}{\nabla b^k}$  in terms of  $\lambda_i^k$  and  $x_i$ . The gradient of the weight matrix  $W$  with respect to the loss for class index  $k$  is given by the average of the gradients over all samples:

$$\nabla W^k = \frac{1}{B} \sum_{i=1}^B \nabla W_i^k \quad (12)$$

According to the chain rule, we can further obtain:

$$\begin{aligned}\nabla W^k &= \frac{1}{B} \sum_{i=1}^B \nabla W_i^k = \frac{1}{B} \sum_{i=1}^B \frac{\partial l(\hat{y}_i^k, y_i)}{\partial \hat{y}_i^k} \cdot \frac{\partial \hat{y}_i^k}{\partial W_i^k} \\ &= \frac{1}{B} \sum_{i=1}^B \frac{\partial l(\hat{y}_i^k, y_i)}{\partial \hat{y}_i^k} \cdot x_i\end{aligned}\quad (13)$$

Similarly, the gradient of the bias corresponding to the  $k^{th}$  category index can be derived as:

$$\begin{aligned}\nabla b^k &= \frac{1}{B} \sum_{i=1}^B \nabla b_i^k = \frac{1}{B} \sum_{i=1}^B \frac{\partial l(\hat{y}_i^k, y_i)}{\partial \hat{y}_i^k} \cdot \frac{\partial \hat{y}_i^k}{\partial b^k} = \frac{1}{B} \sum_{i=1}^B \frac{\partial l(\hat{y}_i^k, y_i)}{\partial \hat{y}_i^k} \cdot 1 \\ &= \frac{1}{B} \sum_{i=1}^B \frac{\partial l(\hat{y}_i^k, y_i)}{\partial \hat{y}_i^k}\end{aligned}\quad (14)$$

Therefore,  $\nabla W^k / \nabla b^k$  can be derived as:

$$\begin{aligned}\frac{\nabla W^k}{\nabla b^k} &= \frac{\frac{1}{B} \sum_{i=1}^B \frac{\partial l(\hat{y}_i^k, y_i)}{\partial \hat{y}_i^k} \cdot x_i}{\frac{1}{B} \sum_{i=1}^B \frac{\partial l(\hat{y}_i^k, y_i)}{\partial \hat{y}_i^k}} = \frac{\sum_{i=1}^B \frac{\partial l(\hat{y}_i^k, y_i)}{\partial \hat{y}_i^k} \cdot x_i}{\sum_{i=1}^B \frac{\partial l(\hat{y}_i^k, y_i)}{\partial \hat{y}_i^k}} \\ &= \frac{\frac{\partial l(\hat{y}_1^k, y_1)}{\partial \hat{y}_1^k} \cdot x_1}{\sum_{i=1}^B \frac{\partial l(\hat{y}_i^k, y_i)}{\partial \hat{y}_i^k}} + \frac{\frac{\partial l(\hat{y}_2^k, y_2)}{\partial \hat{y}_2^k} \cdot x_2}{\sum_{i=1}^B \frac{\partial l(\hat{y}_i^k, y_i)}{\partial \hat{y}_i^k}} + \dots + \frac{\frac{\partial l(\hat{y}_B^k, y_B)}{\partial \hat{y}_B^k} \cdot x_B}{\sum_{i=1}^B \frac{\partial l(\hat{y}_i^k, y_i)}{\partial \hat{y}_i^k}} \\ &= \sum_{i=1}^B \frac{\frac{\partial l(\hat{y}_i^k, y_i)}{\partial \hat{y}_i^k}}{\sum_{j=1}^B \frac{\partial l(\hat{y}_j^k, y_j)}{\partial \hat{y}_j^k}} \cdot x_i.\end{aligned}\quad (15)$$

This expression can be rewritten as:

$$\frac{\nabla W^k}{\nabla b^k} = \sum_{i=1}^B \frac{\frac{\partial l(\hat{y}_i^k, y_i)}{\partial \hat{y}_i^k}}{\sum_{j=1}^B \frac{\partial l(\hat{y}_j^k, y_j)}{\partial \hat{y}_j^k}} \cdot x_i = \sum_{i=1}^B \lambda_i^k \cdot x_i \quad (16)$$

Therefore,  $\lambda_i^k = \frac{\partial l(\hat{y}_i^k, y_i)}{\partial \hat{y}_i^k} / \sum_{j=1}^B \frac{\partial l(\hat{y}_j^k, y_j)}{\partial \hat{y}_j^k}$ , and  $\sum_{i=1}^B \lambda_i^k = 1$  □

## B.2. Proof for Theorem 4.1

*Proof. Continuity of  $L(\theta, \phi)$ :* From Assumption (4.2), since  $\ell(\cdot, \cdot)$  is continuously differentiable with respect to  $\theta$ , the gradient  $\nabla_{\theta} \ell(F(x, \theta), y)$  is continuous with respect to  $\theta$ . The projector  $\Pi$  is a fixed-position sparse sampling linear operator, so the composite function  $\Pi(\nabla_{\theta} \ell(F(x, \theta), y))$  is also continuous with respect to  $\theta$ . By Assumption 4.3, the decoder  $\mathcal{D}$  is continuous. Therefore, the composite function  $\mathcal{D}(\Pi(\nabla_{\theta} \ell(F(x, \theta), y)))$  is continuous with respect to  $\theta$  and  $\phi$ . The squared Euclidean norm  $\|\cdot\|_2^2$  is a continuous. Hence, the loss function  $L(\theta, \phi)$  is continuous with respect to  $\theta$  and  $\phi$ .

**Existence of Global Minimum** From Assumption (4.1) and Assumption (4.3), the parameter space  $\Theta$  and  $\Phi$  is a non-empty compact set. By the Weierstrass Extreme Value Theorem (Rudin, 1976; Bartle & Sherbert, 2011), any continuous function on a compact set attains its maximum and minimum values. Therefore, there exists  $\theta^* \in \Theta$  and  $\phi^* \in \Phi$  such that  $\theta^*, \phi^* = \arg \min_{\theta \in \Theta, \phi \in \Phi} L(\theta, \phi)$ .

**Maximum Vulnerability of the Gradient Space** At  $\theta = \theta^*$  and  $\phi = \phi^*$ , the loss function  $L(\theta, \phi)$  attains its global minimum, which indicates that the reconstruction error is minimized. This indicates that the encoding and decoding processes of the gradient have reached an optimal state. If a better decoder or gradient construction existed, it would further reduce  $L(\theta, \phi)$ , contradicting the minimality of  $L(\theta^*, \phi^*)$ . Therefore, at  $\theta = \theta^*$  and  $\phi = \phi^*$ , the risk of data leakage from the gradient space to the input data  $x$  is maximized. This means the gradient  $\nabla_{\theta} \ell(F(x, \theta^*), y)$  contains the most features of  $x$ , rendering the gradient space most vulnerable. □

### C. More Experimental Evidence

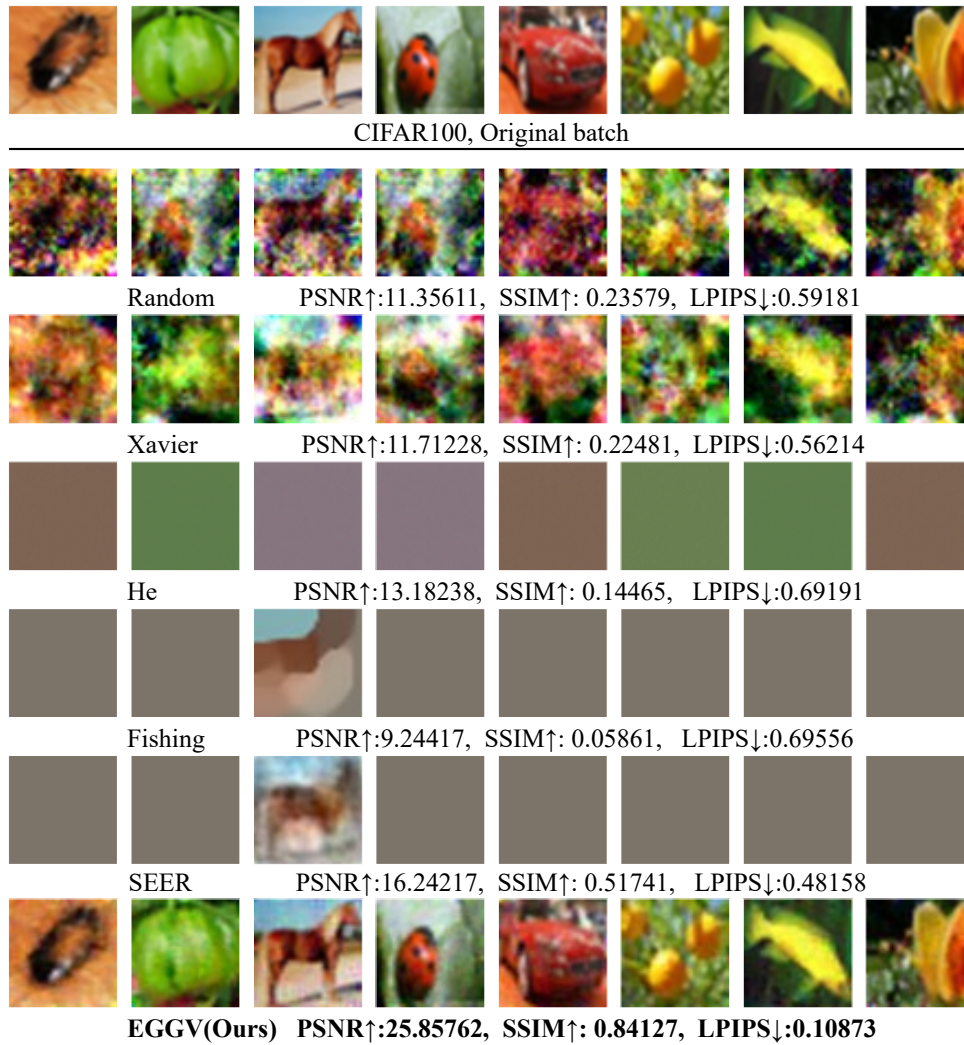


Figure 7. Visual reconstruction of IG on the model with EGGV poisoning, Xavier initialization, and He initialization.